Research Article | Vol. 27, No. 5 | 4 Mar 2019 | OPTICS EXPRESS 6700
Optics EXPRESS

Nanoscopy on-a-chip: super-resolution imaging on the millimeter scale

ØYSTEIN I. HELLE, DAVID A. COUCHERON, JEAN-CLAUDE TINGUELY, CRISTINA I. ØIE, AND BALPREET S. AHLUWALIA*

UiT-The Arctic University of Norway, Klokkargårdsbakken 35, 9037 Tromsø, Norway

*balpreet.singh.ahluwalia@uit.no

Abstract: Optical nanoscopy techniques can image intracellular structures with high specificity at sub-diffraction limited resolution, bridging the resolution gap between optical microscopy and electron microscopy. So far conventional nanoscopy lacks the ability to generate high throughput data, as the imaged region is small. Photonic chip-based nanoscopy has demonstrated the potential for imaging large areas, but at a lateral resolution of 130 nm. However, all the existing super-resolution methods provide a resolution of 100 nm or better. In this work, chip-based nanoscopy is demonstrated with a resolution of 75 nm over an extraordinarily large area of 0.5 mm x 0.5 mm, using a low magnification and high N.A. objective lens. Furthermore, the performance of chip-based nanoscopy is benchmarked by studying the localization precision and illumination homogeneity for different waveguide widths. The advent of large field-of-view chip-based nanoscopy opens up new routes in diagnostics where high throughput is needed for the detection of non-diffuse disease, or rare events such as the early detection of cancer.

1. Introduction

For a long time, the spatial resolution in optical microscopy was believed to be bound by the diffraction limit. The famous resolution equation [1], shows that the resolving power of the microscope is a simple function of numerical aperture (N.A.) and the wavelength of light, effectively limiting the lateral resolution to around 200-300 nm for visible wavelengths. However, from the early 90s up until now a range of techniques developed that aim to produce images with spatial resolution way beyond that of the diffraction limit. This field is commonly known as super-resolution optical microscopy or optical nanoscopy, and has given biologists tools to observe living intracellular structures with unprecedented high resolution. Lately, improvements in the nanoscopy methods have pushed the spatial resolution towards the ultimate limit i.e. the physical size of the fluorescent labels [2]. For conventional immunolabeling at room temperature using antibody-binding of fluorophores, this typically means a few tens of nanometers.

While nanoscopy has pushed the optical resolution, the improvement does not come for free. One of the major payoffs is the reduced size of the field of view (FOV) with images typically being on the size of 10 μm x 10 μm to 50 μm x 50 μm. This severely limits the throughput of the current super-resolution techniques since only parts of a cell, or up to 1-2 cells can be imaged simultaneously. Most of the nanoscopy methods aim to separate the fluorescence molecules in time by manipulating the photo-physics of the fluorescent dye molecules, achieving a spatial resolution down to around 10-30 nm. These techniques include scanning methods such as stimulated emission depletion (STED) [3], and single-molecule localization microscopy (SMLM) methods such as (direct) stochastic optical reconstruction microscopy (d)STORM) [4,5] and (fluorescence) photoactivated localization microscopy ((f)PALM) [6,7]. Methods like stochastical optical fluctuation intensity microscopy (SOFI) [8], entropy-based super resolution imaging (ESI) [9] and multiple signal classification algorithm (MUSICAL) [10] lessen the demand on the control of the photophysics of single-molecules by working with signals from multiple fluorophores and using clever reconstruction algorithms to achieve an improved resolution. One

#345909 https://doi.org/10.1364/OE.27.006700
Journal © 2019 Received 25 Sep 2018; revised 9 Dec 2018; accepted 29 Dec 2018; published 22 Feb 2019

Optics EXPRESS

of the most used methods for live cell imaging is structured illumination microscopy (SIM) [11], which use light pattern illumination to encode high frequency content (unresolved) in low frequency signals, yielding around 100 nm lateral resolution. SIM has gained popularity by its live cell compatibility, minimal photo-toxicity, ease of use, and compatibility with most bright fluorophores.

The next breakthrough in optical nanoscopy would represent high throughput imaging. This refers to techniques that can extend the amount of data acquired, by imaging at super-resolution over large areas/volumes fast. The limited throughput of present day nanoscopy methods hinders the collection of sufficient information for drawing statistically relevant conclusions from biological systems. When looking at extending the field of view of optical nanoscopy the easiest would be to employ SIM and create a stitched image consisting of many SIM images side by side. SIM is inherently fast, since it only use 9 /15 images to create one super resolved SIM image in 2D/3D, and a stitched image can be created in a reasonable amount of time, but with spatial resolution limited to around 100 nm. To get the resolution below 100 nm it is thus necessary to increase the FOV of one of the other nanoscopy techniques. The intrinsic scanning nature of STED makes these techniques slow for large areas (such as 500 μm x 500 μm). On the other hand, SMLM being a wide field method, the entire FOV can be acquired simultaneously which is desirable when moving to large area imaging. SMLM methods are typically not very fast (tens of minutes), since thousands of images needs to be acquired to generate a super-resolved image. However, using advanced reconstruction algorithms including compressive sensing [12], SMLM with high-temporal resolution (i.e. in seconds), has been demonstrated.

To increase the FOV for SMLM images it is desirable to use a low magnification objective lens to cover large areas without scanning. For a given optical set-up, the imaged area acquired for a 20X objective lens will be approximately 10X larger than that of a 60X objective lens. In a conventional SMLM setup, excitation light is sent through a high numerical aperture (N.A.) objective lens, and the emitted fluorescence is detected with the same objective. Using a low magnification and low N.A. objective lens in SMLM will create two problems. Firstly, a low magnification/N.A. objective will have a large depth of field, which scales inversely to N.A. squared. This results in the collection of light signals from rather large volumes, giving increased background signal. This will eventually reduce the localization precision and the optical resolution for SMLM, which relies on 2D Gaussian fits over individual blinking events. Presently this problem is solved by using a high magnification/N.A. total internal reflection fluorescence (TIRF) objective lens. A TIRF lens creates an evanescent field illuminating only a thin section of the sample, typically up to 100-150 nm from the surface and thus generating illumination capable of achieving an excellent signal to noise ratio. However, a low magnification/N.A. TIRF objective lens is not commonly available.

Secondly, the illumination for SMLM needs to be uniform. SMLM relies on sparse blinking of the fluorophores, which for the case of *d*STORM is achieved by photo-switching in the presence of a reducing buffer. An uneven illumination will thus provide un-even switching rates generating poor images. The objective lens generates excitation light with a Gaussian profile, where only the most central part of the FOV is useful for SMLM imaging. A few approaches have improved upon this problem [13, 14], but both methods are still collecting with the same high N.A. objective lens, effectively limiting the FOV.

To alleviate the above mentioned problems, it is evident that the separation of the illumination and collection light paths for SMLM will be beneficial. Recently [15], it was shown that by using a photonic chip to illuminate the specimen one could use low magnification objectives to acquire *d*STORM images over an area of 500 μm x 500 μm, 100X larger area than the conventional approach, with lateral resolution of 130 nm.

However, in the previous work the resolution demonstrated by chip-based *d*STORM was limited to around 130 nm and thus could not surpass the diffraction barrier of 100 nm. With a

Optics EXPRESS

resolution of 130 nm chip-based *d*STORM lacked the impact over SIM which can acquire slightly better resolution (100-120 nm) over the same area by scanning and stitching in less time than chip based *d*STORM. In this paper we show that chip-based *d*STORM can be used to acquire images with an optical resolution of 70-75 nm over an extra-ordinary large FOV (500 μm x 500 μm), and thus breaking the diffraction barrier of 100 nm for high throughput optical nanoscopy. Here, we have also investigated crucial parameters to benchmark the performance of chip-based nanoscopy such as localization precision as a function of waveguide width and input power; and the uniformity of the illumination generated by the chip as a function of waveguide width.

2. Principle of chip-based fluorescence imaging

In conventional microscopy/nanoscopy the sample is prepared on a glass-slide/coverslip. Chip-based microscopy replace this arrangement with a photonic integrated circuit (PIC) and the sample is prepared directly on the PICs top surface, as depicted in Fig. 1(a). The PIC chip is made on a Silicon substrate with a buffer layer of Silicon Dioxide (SiO_2) followed by a thin top layer of Silicon Nitride (Si_3N_4). By shaping the geometry, i.e creating side-walls, the layer functions as as an efficient waveguide for propagating excitation light to the specimen. Laser-light is coupled into the waveguide by focusing a beam of light on to the end-facet using an objective lens. The light propagates inside the waveguide by total internal reflection, however a small part the field leaks out in the form of an evanescent wave. The specimen is fluorescently labeled and the fluorophores are excited via the evanescent field stretching around 150 nm in to the sample as shown i Fig. 1(b). This means that only the part of the specimen located within these 150 nm will be illuminated. The evanescent field penetration depth is fully determined by the wavelength, and the local refractive index at the waveguide-sample boundary. The sample can be mounted following the same protocols as for the glass-slide/coverslip arrangement, and the PIC has also shown to be bio-compatible supporting live cells experiments [16].

For efficient photo-switching of the fluorophores, the evanescent field intensity directly at the surface must be strong (ideally 1-10 kW/cm^2), which is achieved by the use of a high refractive index material, in this work Si_3N_4 having n$\approx$ 2.0, for 660 nm excitation laser light. The high-refractive index material together with a shallow cross-section (waveguide thickness of 150 nm) confines the light tightly inside the waveguide, but with up to 5-10% of the guided power available in the evanescent field. The high refractive index contrast also ensure that the penetration depth of the evanescent field is shallow, yielding good optical sectioning.

Using a high-refractive index waveguide such as Si_3N_4 at visible wavelengths, higher order modes are supported by the strip waveguide geometry starting from waveguide widths of 1.5 μm. These modes travel in discrete paths generating non-uniform illumination patterns. As the dimensions increase above a few micrometers, more modes starts to interfere with each other, creating a highly chaotic illumination pattern, referred to as multi-mode interference (MMI) patterns. The resulting evanescent field illumination is thus also contaminated with non-uniform MMI patterns, resulting in images of poor quality, disturbed by stripe patterns. The MMI patterns can be scrambled, and thus create a uniform image by shifting the mode patterns in time, and then take the average of several sub-sets of MMI patterns. There are two possibilities to achieve this, either rapid scanning the input beam using a galvo mirror, or slow scanning the input beam by moving the coupling objective lens using a motorized/piezo stage. The galvo mirror can scan quicker than the camera exposure time so every frame captured will show uniformity. The other approach scans slowly, using the average of a few hundred frames to create a uniform image. In the case of *d*STORM several thousand frames are captured by default so any of the two methods can be used. In this paper we chose to slow-scan the input beam by moving the coupling objective with a piezo stage as discussed in [15].

Unlike the TIRF objective lens, the generation of the evanescent field by an optical waveguide is decoupled from the imaging objective lens. As a consequence, the evanescent field is available

Optics EXPRESS

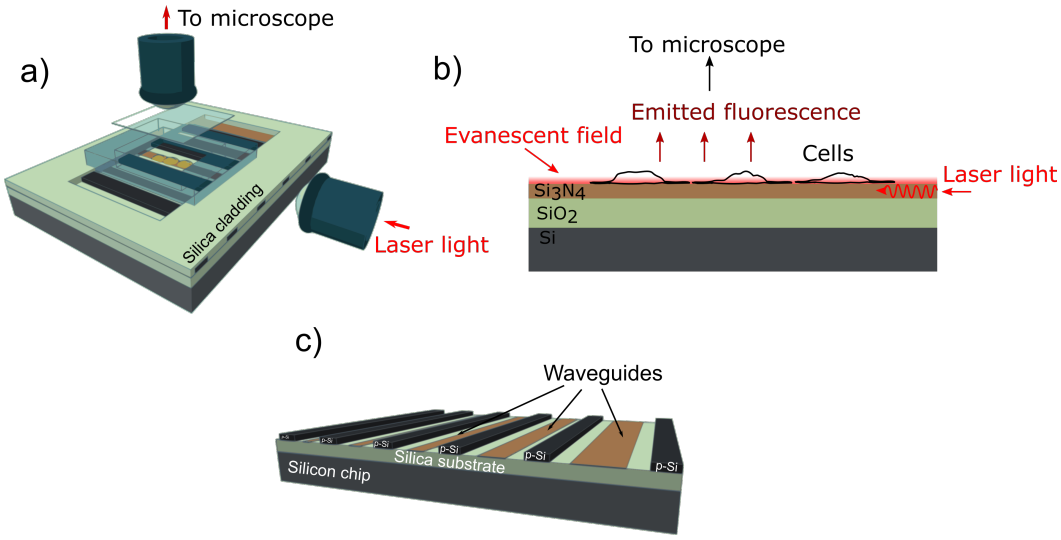

Fig. 1. a) Laser light is coupled into a PIC via an objective lens, and light is guided towards the specimen in optical waveguides. On top of the chip there is a PDMS microchamber to contain the image buffer. b) In the center of the chip there is an opening in the protective cladding where the specimen is mounted to come in contact with the evanescent field. The fluorescent signal is captured by an upright microscope. c) The PIC has lateral dimension of around 3 cm x 3 cm. A layer of SiO_2 give a strong refractive index contrast against the Si_3N_4 waveguide. In between the guiding material are layers of Poly-Silicon that blocks light from passing in to neighboring waveguides.

over large areas, only limited by the waveguide dimension. Furthermore, it allows a free choice of the objective lens used to collect the emitted fluorescence. In this way, a low N.A. objective lens can be used to acquire a large FOV without sacrificing the excellent optical sectioning provided by the chip-based illumination.

3. Materials and methods

3.1. Waveguide fabrication

The waveguides were made by first sputtering a 2 μm thick layer of SiO_2 onto a silicon wafer. The 150 nm thick guiding layer of Si_3N_4 was then added by low-pressure chemical vapor deposition at 800°C, before the waveguide structure was outlined by photo-lithography. The strip waveguide structures were then realized by ion etching all the way down to the silica cladding. Another layer of poly-silicon was realized to function as a light absorbing layer in between neighboring waveguides to stop unguided light from leaking to other waveguides. This can be seen as the black layer in Fig. 1(c). A 1.5 μm thick layer of SiO_2 was used to create a protective top cladding, and reactive ion etching was used to open up the cladding at the imaging area, where cells can be seeded directly on top of the waveguide core accessing the evanescent field. For fluorescence imaging of biological samples, the dimensions typically must be larger than the cells under investigation. Here, waveguide widths between 50 μm and 1 mm were used. A PDMS micro-chamber was used to contain the aqueous image buffer during the measurements. The thickness of the chamber was approximately 130 μm, well below the working distance of the objective lens used for the collection.

Optics EXPRESS

3.2. Experimental setup

The setup was based around an Olympus modular upright microscope fitted with a water cooled sCMOS camera (Hamamatsu ORCA flash). Images were acquired using two different objective lens (Olympus UplanSApo x60/1.2 w and Zeiss LD LCI Plan-Apochromat x25/0.8). The Zeiss multi-immersion objective lens was used to gather the large FOV images. The Zeiss objective lens was used with the olympus tube lens, such that the effective magnification of the setup changed, leaving around 27 x effective magnification. The chip was secured by a vacuum air-lock to further minimize sample drift. Laser was coupled into the chip using a x50/0.8 objective lens. The laser used for *d*STORM is a Cobolt Flamenco 660 nm with up to 500 mW output power. The microscope was mounted on motorized stages enabling lateral movement for observation of different regions on the chip. The data was acquired using a computer and the localization data was analyzed using Fiji open source image processing software and the localization data analysis plugin ThunderStorm [17]. The camera exposure time was set to 25 ms for all *d*STORM experiments.

3.3. Sample preparation

A fluorescently labeled surface was created by incubating a solution of 50nM Alexa647 molecules in 0.05% Poly-L-Lysine for 10 minutes at room temperature (RT). The solution was aspirated and the surface rinsed gently three times with dH20. *d*STORM buffer was prepared following [18]. The buffer contains an enzymatic scavenger system containing Catalase (Sigma #C100) and Glucose Oxidase(Sigma #G2133) together with 100 mM Mercaptoethylamine (MEA, Sigma #M6500). The addition of 2mM Cyclotetraene (COT, Sigma #138924) has shown to help with blinking performance of Alexa647 on waveguides. Cells were harvested from male Sprawgly rat, with body weights between 150-300 g. Liver sinusoidal endothelial scavenger cells were isolated using the method from [19], and kept alive in RPMI 1640. To help with attaching the cells to the waveguides chips, the surface was coated with fibronectin (50 μg/ml) for 10 minutes at RT. The cell suspension was incubated on the surface of the chips for 1 hour at 37°C and 5% O_2. The surface was rinsed with fresh RPMI 1640, to remove debris and the chips were incubated for 2 more hours to allow spreading of the cytoplasm. Fixation of the cells were performed using 4% Paraformaldehyde for 30 min. The tubulin was stained using primary antibody β-tubulin(Sigma Aldrich) at 1:400 in PBS for 1h at RT. The secondary antibody was goat anti-mouse Alexa Fluor 647 at 1:400 in PBS, incubated for 1H at RT. The cells were washed three times with PBS before the image buffer was applied and the chambers sealed with a coverglass.

4. Results

For high throughput chip-based nanoscopy, wide waveguides are essential to illuminate large areas. The dimensions of the waveguides must be made such that the evanescent field intensity is sufficiently strong, enabling photo-switching of fluorophores on top of the waveguide surface. In order to establish the appropriate waveguide dimensions for large FOV imaging we investigate the impact of waveguide width and input power for a *d*STORM on-chip measurement. This was achieved by measuring localizations coming from a single-molecule layer deposited on top of the waveguide surface, as a function of waveguide widths and at different input powers. A *d*STORM experiment was carried out on the surface over a fixed area, and repeated for different waveguide widths. Waveguides of different widths were located next to each other on the same chip as indicated in Fig. 1(a). In Fig. 2 the number of localizations acquired using 1000 frames of data is plotted against the input power for 4 different waveguide widths. The number of localizations detected for each waveguide width follow the same trend for waveguide widths up to 400 μm, while for the 600 μm wide waveguide the curve takes on another shape. This shows that waveguides of widths 200-400 μm generate an evanescent field suitable to efficiently

Optics EXPRESS

photo-switch the fluorophores with an input power of 25 mW. While, for the 600 μm waveguide, 100 mW input power is needed to get the maximum number of localized emitters for a similar imaging area.

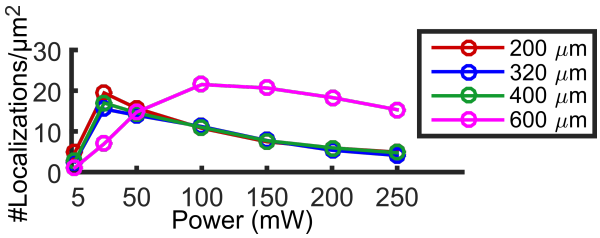

Fig. 2. Localizations as a function of power and width – The average number of localizations over a fixed area for different waveguide widths and input powers. We see that for waveguides 200 - 400 μm wide around 25 mW at the input of the waveguide is enough to get optimum blinking, while for 600 μm waveguide we must increase the power to 100mW.

To systematically investigate the achievable uniformity of chip-based illumination, we measured the intensity profiles acquired by staining the waveguide surface with a dense thin layer of fluorophores (Alexa 647 in Poly-L-Lysine) and diffraction limited imaging by using mode averaging. In Fig. 3(a) the MMI pattern is shown without using mode averaging, while in Fig. 3(b) the same area is imaged after mode averaging. The line-profile in Fig. 3(b) indicate the position from where the modulation depths for different waveguide widths are calculated. The measured modulation depth for waveguide widths stretching between 120 μm up to 1000 μm are shown in Fig. 3(c) using 500 frames of data, with Fig. 3(d) showing the line-profile from Fig. 3(b) as an example. When calculating the modulation depth, the edge artifacts observed in Fig. 3(d) are neglected. Interestingly, it was observed that the modulation depth for these dimensions are rather stable in terms of being viable for *d*STORM imaging, with around 17 % for the 120 μm and up to 27 % for 1000 μm wide waveguides.

We demonstrate the method by imaging liver sinusoidal endothelial cells (LSECs) stained for the micro-tubules network. The *d*STORM localization list was filtered to only keep the localizations with the best statistics, like brightness and shape, ensuring that few overlapping emitters introduce errors for the fitting algorithm. The number of images used to compile the reconstructed image was around 25000 selected from a stack of 65000 images acquired. The image shown in Fig. 4(a) show that by using the 25x 0.8 N.A. objective lens an extremely large area of almost 500 μm x 500 μm with a resolution down to 70-75 nm can be imaged. The large area illuminated by the waveguide allow 200-300 cells to be imaged simultaneously. The zoom in Fig. 4(b) show the comparison to the diffraction limited image visualizing a 6-fold resolution enhancement of the 25x 0.8 N.A objective lens. In Fig. 4(c) the zoom also indicates the position of the lineplot in Fig. 4(d) which show a clear separation of tubulin filaments located 78 nm apart. In Fig. 4(e), this resolution is confirmed using Fourier ring correlation [20], which suggest a lower threshold for the resolution over the entire image to be around 72 nm. Furthermore, we see that the average localization precision in the image, as measured by the reconstruction software is peaking around 23 nm (Fig. 4(f)), indicating a lower limit for the resolution of around 65 nm.

It can be noticed from Fig. 4(a) that a slight decay in the number of localized molecules towards the edges of the image, which is caused by the limited field flatness of the imaging objective lens. To study the influence of field flatness of the imaging objective lens, we investigated the achieved localization precision as a function of position in the field of view. As it can be seen from Fig. 3(c), the waveguides can set up an evanescent field where the intensity modulation depth is around 25 % for large fields of view. However, when producing really large high-resolution images we are still limited by the collection optics. Microscope objectives with high numerical aperture

Optics EXPRESS

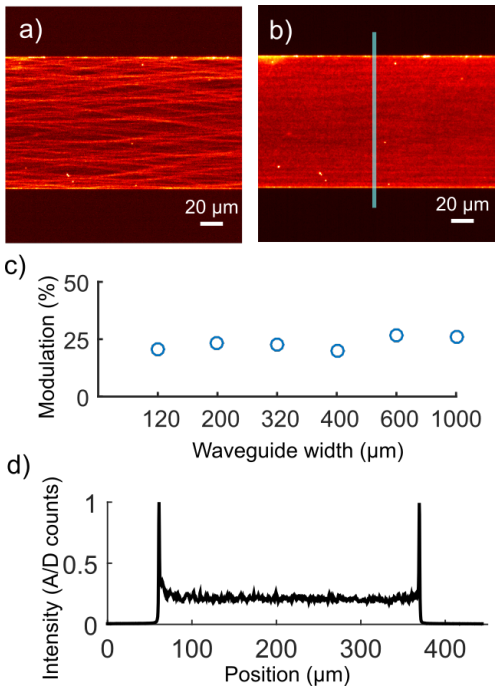

Fig. 3. Modulation depth as function of waveguide width – a) Illumination MMI pattern without mode averaging. b) After mode averaging the resulting illumination is close to uniform. c) The modulation depth is plotted for different waveguide widths, and only small changes is observed when the width increases. d) The line-profile indicated in b). When calculating the modulation depth the edge artifacts are ignored.

and low magnification are not very common, and the ones that do exists typically have to pay the price for these unusual characteristics in terms of field flatness. Most microscope objectives expressing these characteristics give a nice focus only in the middle of the FOV. Fig. 5 shows the localizations from the image in Fig. 4(a) grouped in bins of 10 μm along x (horizontally) but with the full field-of-view along y (vertically). The number of localization detected for each bin is displayed, visualizing how the number of localizations decrease when moving away from the center. The likelihood of acquiring a good localization is decreasing when the emitter is laying in the periphery of the FOV, which means that either we need to accept a decrease in resolution (keeping less good localizations), or we need to increase the acquisition time to allow enough localizations to be captured to fully resolve the structures at acceptable resolution.

5. Discussion and conclusion

Super-resolution microscopy has so far come at the cost of throughput. Currently, commercial setups provide unprecedented resolution but the size of the field of view is small, with images typically covering only parts of a cell. This is a consequence of conventional setups being bound to a high N.A. and high magnification objective lens for both the illumination and the collection. To make use of optical nanoscopy to study statistical biological nanometer sized phenomenon on large length scales, the need to increase the throughput of the methods is apparent. In this study we used planar optical waveguides as a mean to illuminate fluorescently labeled specimen located on top of the waveguide surface via intrinsic evanescent fields. This method of exciting fluorescence via planar waveguides allows for TIRF optical nanoscopy with the additional feature of a free choice of the imaging objective lens, allowing scalable super-resolution microscopy

Optics EXPRESS

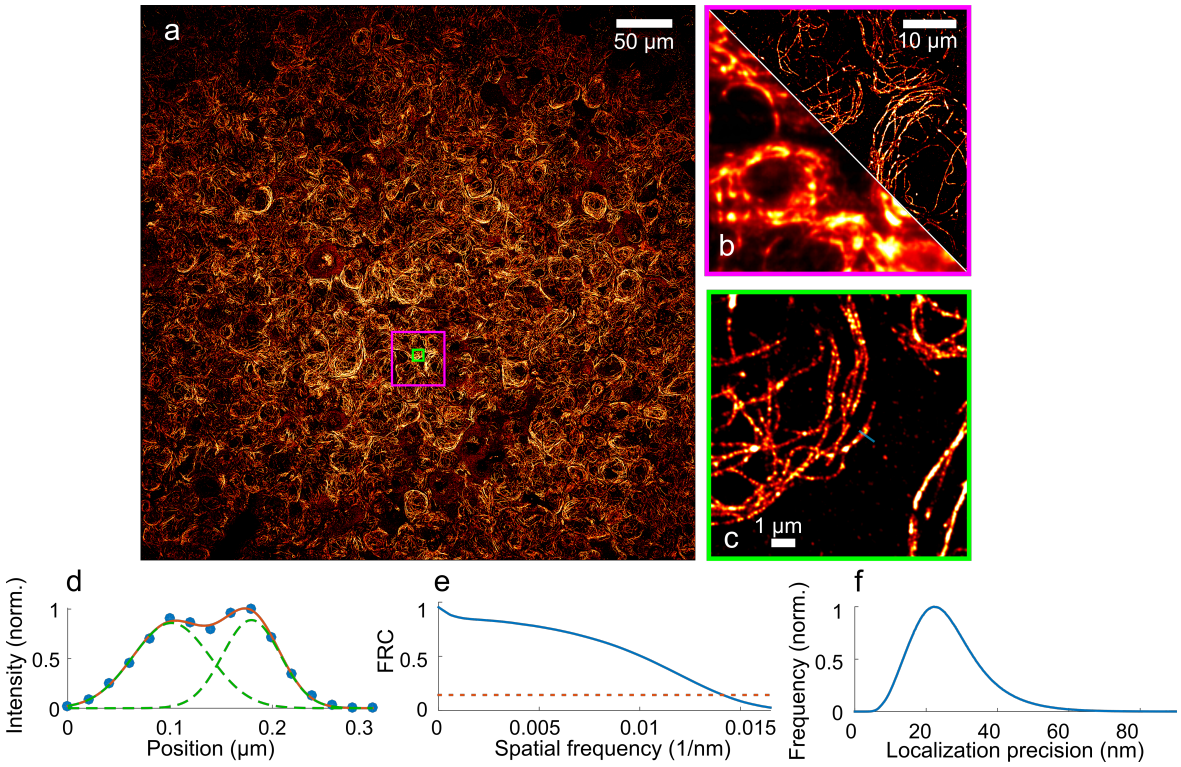

Fig. 4. a) Large field of view *d*STORM image of Alexa 647 stained tubulin in rat L SECs. The image has a resolution of around 70-75 nm with 200-300 cells being imaged simultaneously. b) Zoomed image from a) with comparison to the diffraction limited image. c) Zoomed image marked in green from a) with the position of the lineplot shown in d) marked. d) The lineplot show tubulin filaments clearly separated by a distance of 78 nm. e) Fourier ring correlation indicated a resolution of around 72 nm. f) The localization precision measured by the reconstruction software further backs a resolution between 70-75 nm.

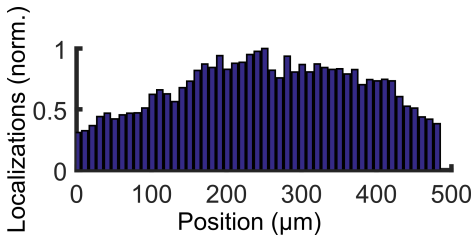

Fig. 5. Localizations from Fig. 4 as function of width across the field of view. Each data point includes all localizations within a bin width of 10μm horizontally separated . We see that the number of properly localized molecules decrease moving away from the center of the objective lens.

Optics EXPRESS

with a compromise between FOV size and resolution.

Compared to the standard coverglass/glass slide arrangement, the PIC chips are more expensive to make. However, when mass produced using CMOS fabrication processes and in a foundry the price per chip can be reduced significantly. The price range of a few dollars per millimeter square can easily be achieved during industrialized production. As the price for silicon wafers scales with the chip area, hosting a small chip (e.g. 2 x 2 mm^2) inside a plastic holder could be an alternative for easy handling of the chip.

The previously published results [15] using the chip-based approach greatly enhanced the size of the field of view available for nanoscopy imaging, but with the resolution not exceeding more than 130 nm. In this work, we show that the method is capable of generating images with 70-75 nm resolution, by carefully selecting the objective lens used in the image acquisition. The increased resolution surpasses the possible 100 nm resolution achievable using SIM. Other previously reported techniques [13, 14] on increased FOV SMLM have achieved a more uniform excitation light spanning over a larger area, but they are still limited by the high N.A. objective lens for acquiring the emitted fluorescence, effectively limiting the FOV to around 200 μm x 200 μm at best.

Furthermore, we investigated how the blinking of fluorophores on waveguides react to different parameters such as waveguide width and laser intensity. As seen from Fig. 2, the switching rates was at its best at 25 mW input power using a single molecule surface with widths of 200-400 μm but a 4 times increase in power was needed to get equally good blinking from a 600 μm waveguide. The surface intensity scales with the width of the waveguide, justifying the need for more input power at 600 μm width, but other factors like coupling efficiency could also impact the curves of Fig. 2. It has been shown that Alexa 647 exhibits faster switching kinetics at high powers [21]. The drop in the number of localizations found above 25 mW (for 200-400 μm) and 100 mW (for 600 μm) could indicate that the fluorophores are blinking much faster than the exposure time of the camera giving increased background. It might also be that the increased intensity is pushing more fluorophores in to more long lived dark-states or to a permanent off-state by photo-bleaching. In either case, laser powers above 25 mW is too strong for efficient SMLM on waveguides using the *d*STORM method, and that the surface intensity is higher than earlier estimates [15], where it was shown that an input laser power of 500 mW yielded up to 10kW/cm^2 evanescent field intensity. From experimental data using cells we have experienced that the intensity needed to efficiently photo-switch Alexa 647 must be scaled up a few times to achieve adequate blinking in cells. This is probably due to fluorophores sitting tens of nanometers or more away from surface in case of cells, while the illumination is exponentially decaying away from the surface.

The modulation depth of the resulting illumination pattern after mode averaging was studied. In *d*STORM imaging the modulation depth plays a role in terms of the pattern being viable for use with the *d*STORM technique. As long as there is sufficient intensity to effectively photo-switch the fluorophores, the modulation has little impact. However if intensity reduces in some regions to such an extent that the photo-switching is affected, this can create a problem. For waveguides of 120 μm a modulation depth of 17% which corresponds well with earlier investigations, and for wider waveguides we see that the number increase to 25-30%. When looking at the *d*STORM image of Fig. 4(a) we see that this plays little role in the end result. However, the temporal resolution might be reduced if the modulation is decreased, in that more fluorophores in general will be in the desired on/off state at each instance. To reduce the modulation index for wide waveguides the scan range could be increased to scan over the entire input width, contrary to 20μm as achieved here. The waveguide could also start at a lower width, and taper out to wide dimension to reduce the need for larger scan range.

The chip-based platform also supports different on-chip optical modalities such as Raman spectroscopy on chip [22], on-chip micro-particle manipulation [23], interferometric microparticle

Optics EXPRESS

sensing [24] and gas sensing [25], where several of these techniques can be combined creating advanced lab-on-a-chip multimodality platforms. In this work, we have investigated the relationship between waveguide widths and some parameters related to extending the FOV in super-resolution microscopy imaging. By using the waveguide-chip we have by-passed the need of a conventional objective lens to generate the excitation light, however we still reply on using an objective lens to collect the fluorescence s ignal. The impact of chip-based nanoscopy will be further enhanced if we can replace the objective lens with a micro-lens array to collect the fluorescence s ignal. Such a system will not only be highly compact [26] but will also benefit from the extra-ordinary large illumination area as the waveguide can excite fluorescence along its entire length. Furthermore, the resolution of chip-based SMLM is determined by the SNR of the detected single-molecule emissions. By using brighter emitters the resolution can be further improved, e.g using DNA-paint probes [27], where a fluorophore in the ideal case emits all of its photons in one localization event, thus improving the localization precision.

Large field of view nanoscopy will be useful in diagnostic pathology [28]. For non-diffusive diseases, large areas need to be scanned looking for rare events like cancer cells. Pathology mainly focus on thin tissue sections either 4 μm paraffin embedded samples or 100-200 nm cryo-preserved tissue samples. Thin tissue sections are perfectly matched for the large area TIRF illumination produced by the chip-based imaging technology and will be explored in future work.

Funding

European Research Council, project number 336716.

Acknowledgments

This work has made use of the Spanish ICTS Network MICRONANOFABS partially supported by MEINCOM.

References

1. J. Goodman, *Introduction to Fourier Optics* (Roberts & Company, 2005), pp. 156–160.
2. S. Weisenburger, D. Boening, B. Schomburg, K. Giller, S. Becker, C. Griesinger, and V. Sandoghdar, "Cryogenic optical localization provides 3d protein structure data with angstrom resolution," Nat. Methods **14**, 141–144 (2017).
3. S. W. Hell and J. Wichmann, "Breaking the diffraction resolution limit by stimulated emission: stimulated-emission-depletion fluorescence microscopy," Opt. Lett. **19**, 780–782 (1994).
4. M. Heilemann, S. van de Linde, M. Schüttpelz, R. Kasper, B. Seefeldt, A. Mukherjee, P. Tinnefeld, and M. Sauer, "Subdiffraction-resolution fluorescence imaging with conventional fluorescent probes," Angew. Chem. Int. **47**, 6172–6176 (2008).
5. M. J. Rust, M. Bates, and X. Zhuang, "Sub-diffraction-limit imaging by stochastic optical reconstruction microscopy (storm)," Nat. Methods **3**, 793–796 (2006).
6. S. T. Hess, T. P. K. Girirajan, and M. D. Mason, "Ultra-high resolution imaging by fluorescence photoactivation localization microscopy," Biophys. J. **91**, 4258–4272 (2006).
7. E. Betzig, G. H. Patterson, R. Sougrat, O. W. Lindwasser, S. Olenych, J. S. Bonifacino, M. W. Davidson, J. Lippincott-Schwartz, and H. F. Hess, "Imaging intracellular fluorescent proteins at nanometer resolution," Science **313**, 1642–1645 (2006).
8. T. Dertinger, R. Colyer, G. Iyer, S. Weiss, and J. Enderlein, "Fast, background-free, 3d super-resolution optical fluctuation imaging (sofi)," Proc. Natl. Acad. Sci. U.S.A **106**, 22287–22292 (2009).
9. I. Yahiatene, S. Hennig, M. Müller, and T. Huser, "Entropy-based super-resolution imaging (esi): From disorder to fine detail," ACS Photonics **2**, 1049–1056 (2015).
10. K. Agarwal and R. Macháň, "Multiple signal classification algorithm for super-resolution fluorescence microscopy," Nat. Commun. **7**, 13752 (2016).
11. M. G. Gustafsson, "Surpassing the lateral resolution limit by a factor of two using structured illumination microscopy," J. Microsc. **198**, 82–87 (2000).
12. L. Zhu, W. Zhang, D. Elnatan, and B. Huang, "Faster storm using compressed sensing," Nat. Methods **9**, 721–723 (2012).
13. J. Deschamps, A. Rowald, and J. Ries, "Efficient homogeneous illumination and optical sectioning for quantitative single-molecule localization microscopy," Opt. Express **24**, 28080–28090 (2016).

Optics EXPRESS

14. A. Beghin, A. Kechkar, C. Butler, F. Levet, M. Cabillic, O. Rossier, G. Giannone, R. Galland, D. Choquet, and J.-B. Sibarita, "Localization-based super-resolution imaging meets high-content screening," Nat. Methods **14**, 1184–1190 (2017).
15. R. Diekmann, Ø. I. Helle, C. I. Øie, P. McCourt, T. R. Huser, M. Schüttpelz, and B. S. Ahluwalia, "Chip-based wide field-of-view nanoscopy," Nat. Photonics **11**, 322–328 (2017).
16. J.-C. Tinguely, Ø. I. Helle, and B. S. Ahluwalia, "Silicon nitride waveguide platform for fluorescence microscopy of living cells," Opt. Express **25**, 27678–27690 (2017).
17. M. Ovesný, P. Křížek, J. Borkovec, Z. Švindrych, and G. M. Hagen, "Thunderstorm: a comprehensive imagej plug-in for palm and storm data analysis and super-resolution imaging," Bioinformatics **30**, 2389–2390 (2014).
18. S. van de Linde, A. Löschberger, T. Klein, M. Heidbreder, S. Wolter, M. Heilemann, and M. Sauer, "Direct stochastic optical reconstruction microscopy with standard fluorescent probes," Nat. Protoc. **6**, 991–1009 (2011).
19. B. Smedsrød and H. Pertoft, "Preparation of pure hepatocytes and reticuloendothelial cells in high yield from a single rat liver by means of percoll centrifugation and selective adherence," J. Leukoc. Biol. **38**, 213–230 (1985).
20. N. Banterle, K. H. Bui, E. A. Lemke, and M. Beck, "Fourier ring correlation as a resolution criterion for super-resolution microscopy," J. Struct. Biol. **183**, 363–367 (2013).
21. Y. Lin, J. J. Long, F. Huang, W. C. Duim, S. Kirschbaum, Y. Zhang, L. K. Schroeder, A. A. Rebane, M. G. M. Velasco, A. Virrueta, D. W. Moonan, J. Jiao, S. Y. Hernandez, Y. Zhang, and J. Bewersdorf, "Quantifying and optimizing single-molecule switching nanoscopy at high speeds," PloS one **10**, e0128135–e0128135 (2015).
22. P. C. Wuytens, A. G. Skirtach, and R. Baets, "On-chip surface-enhanced raman spectroscopy using nanosphere-lithography patterned antennas on silicon nitride waveguides," Opt. Express **25**, 12926–12934 (2017).
23. Ø. I. Helle, B. S. Ahluwalia, and O. G. Hellesø, "Optical transport, lifting and trapping of micro-particles by planar waveguides," Opt. Express **23**, 6601–6612 (2015).
24. F. T. Dullo and O. G. Hellesø, "On-chip phase measurement for microparticles trapped on a waveguide," Lab Chip **15**, 3918–3924 (2015).
25. F. T. Dullo, S. Lindecrantz, J. Jágerská, J. H. Hansen, M. Engqvist, S. A. Solbø, and O. G. Hellesø, "Sensitive on-chip methane detection with a cryptophane-a cladded mach-zehnder interferometer," Opt. Express **23**, 31564–31573 (2015).
26. A. Orth and K. Crozier, "Gigapixel fluorescence microscopy with a water immersion microlens array," Opt. Express **21**, 2361–2368 (2013).
27. J. Schnitzbauer, M. T. Strauss, T. Schlichthaerle, F. Schueder, and R. Jungmann, "Super-resolution microscopy with dna-paint," Nat. Protoc. **12**, 1198–1228 (2017).
28. F. Herrmannsdörfer, B. Flottmann, S. Nanguneri, V. Venkataramani, H. Horstmann, T. Kuner, and M. Heilemann, *3D dSTORM Imaging of Fixed Brain Tissue* (Springer New York, 2017), pp. 169–184.